

**PREPARED FOR THE U.S. DEPARTMENT OF ENERGY,  
UNDER CONTRACT DE-AC02-76CH03073**

**PPPL-3525**

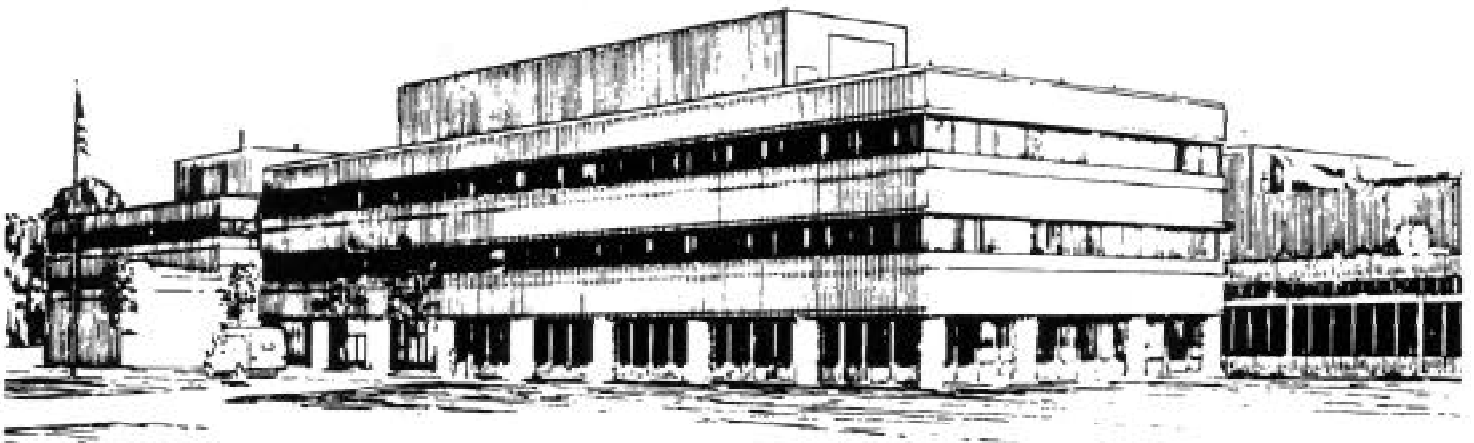
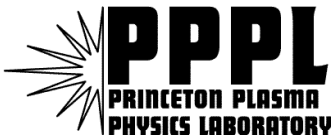
**PPPL-3525**

**Energetic Ion Loss Diagnostic for the Wendelstein 7-AS Stellarator**

**by**

**D.S. Darrow, A. Werner, and A. Weller**

**December 2000**



**PRINCETON PLASMA PHYSICS LABORATORY  
PRINCETON UNIVERSITY, PRINCETON, NEW JERSEY**

## **PPPL Reports Disclaimer**

This report was prepared as an account of work sponsored by an agency of the United States Government. Neither the United States Government nor any agency thereof, nor any of their employees, makes any warranty, express or implied, or assumes any legal liability or responsibility for the accuracy, completeness, or usefulness of any information, apparatus, product, or process disclosed, or represents that its use would not infringe privately owned rights. Reference herein to any specific commercial product, process, or service by trade name, trademark, manufacturer, or otherwise, does not necessarily constitute or imply its endorsement, recommendation, or favoring by the United States Government or any agency thereof. The views and opinions of authors expressed herein do not necessarily state or reflect those of the United States Government or any agency thereof.

## **Availability**

This report is posted on the U.S. Department of Energy's Princeton Plasma Physics Laboratory Publications and Reports web site in Calendar Year 2000. The home page for PPPL Reports and Publications is: [http://www.pppl.gov/pub\\_report/](http://www.pppl.gov/pub_report/)

DOE and DOE Contractors can obtain copies of this report from:

U.S. Department of Energy  
Office of Scientific and Technical Information  
DOE Technical Information Services (DTIS)  
P.O. Box 62  
Oak Ridge, TN 37831  
  
Telephone: (865) 576-8401  
Fax: (865) 576-5728  
Email: [reports@adonis.osti.gov](mailto:reports@adonis.osti.gov)

This report is available to the general public from:

National Technical Information Service  
U.S. Department of Commerce  
5285 Port Royal Road  
Springfield, VA 22161  
  
Telephone: 1-800-553-6847 or  
(703) 605-6000  
Fax: (703) 321-8547  
Internet: <http://www.ntis.gov/ordering.htm>

# **Energetic Ion Loss Diagnostic for the Wendelstein 7-AS Stellarator**

D. S. Darrow,

Princeton Plasma Physics Laboratory, Princeton, NJ, USA

A. Werner, and A. Weller,

Max Planck Institut für Plasmaphysik, Garching, Germany

## **Abstract**

A diagnostic to measure the loss of energetic ions from the Wendelstein 7-AS (W7-AS) stellarator has been built. It is capable of measuring losses of both neutral beam ions and energetic ions arising from ion cyclotron resonant heating. The probe can measure losses of both clockwise and counterclockwise-going energetic ions simultaneously, and accepts a wide range of pitch angles in both directions. Initial measurements by the diagnostic are reported.

## I. Introduction

As stellarators of near reactor size are constructed and operated [1, 2], the issues of how efficient auxiliary heating is and how well alpha particles would be confined grow in importance. Since neutral beam (NB) heating and ion cyclotron resonant heating (ICRH) both result in sizable populations of energetic ions (i.e. with energies at least several times the typical thermal particle energy), the fraction of energetic ions which are lost under a variety of plasma conditions is linked directly with the issue of the efficiency of plasma heating. In addition, the loss of energetic ions from the plasma can produce localized heating of plasma facing components. In extreme cases, losses could damage such components. While the energetic ion confinement properties of a number of stellarator configurations have been studied theoretically [6-8], there have been relatively few measurements of this loss rate [5]. For these reasons, we have built and started operation of a diagnostic to measure the energetic ion loss rate from W7-AS plasmas. While the diagnostic measures losses only at one location on the wall, the data it provides are sufficiently detailed to test existing or proposed models of beam ion losses in W7-AS.

The W7-AS stellarator [9,10] is a low shear stellarator with a major radius of  $R=2$  m, average minor radius of  $\langle a \rangle = 0.2$  m, five field periods, and typically operates with  $n_e = 0.1 - 2 \times 10^{20} \text{ m}^{-3}$ ,  $T_e < 6$  keV, and  $T_i < 1.5$  keV. W7-AS plasmas typically have a rotational transform near  $1/3$  or  $1/2$ . Plasmas are generated in hydrogen and deuterium, and can be heated with 1.5 MW of electron cyclotron resonance heating (ECRH), 1 MW of ICRH,

and up to 3 MW of NB injection. The neutral beams are injected at an energy of 55 keV (for deuterium) or 50 keV (for hydrogen). The NB injectors are arranged in two units of four beam sources each, injecting in opposite directions. The beams which are co-injecting (velocity vector approximately antiparallel with respect to the direction of the B-field) are designated E1-E4. The counter-injecting beams (velocity vector approximately parallel to B) are designated W1-W4. Figure 1 shows a top view of the W7-AS device, the location of NB injectors, and the position of the energetic ion loss probe.

## II. Orbit classes

In classical stellarators, orbits can be classified as passing or trapped, and trapped orbits themselves can be subdivided into toroidally-trapped (bananas), helically-trapped orbits, or a combination of both (superbananas). In W7-AS, however, a classification of such orbits is much more complicated since, due to the modular field coils, the poloidal and helical field ripple are not the only dominating ones. The objective of this section is to demonstrate that a classification of energetic ions in W7-AS into passing and trapped is sufficient. For ions at the beam injection energy in W7-AS, trapped orbits are most probably lost to the walls.

In Fig. 2, real orbits of 50 keV and 5 keV  $H^+$  in a vacuum field configuration with  $\iota=0.34$  are depicted as an example. The guiding centers of the real orbits are transformed into magnetic coordinates and the  $B_{\text{mod}}$  structure at approximately half the minor plasma

radius is shown as well. In the case of 5 keV ions, passing, trapped banana, and trapped loss orbits can easily be found. The banana orbit is also precessing toroidally, and the ions are trapped in the poloidal field ripple. Other orbits can also occur, which cannot be assigned to a specific orbit class, and only a classification may be applied as given by Dettrick *et al* [7], where the number of local maxima in parallel kinetic energy between bounce points are counted. In general, ion orbits in W7-AS exhibit a very individual behavior caused by the large number of non-negligible high Fourier harmonics of the magnetic field structure.

In the case of energetic ions, the classification is clearer because the banana width is larger ( $\sim \rho/\iota$ , where  $\rho$  is the gyroradius and  $\iota$  is the rotational transform) and it is much more probable that such ions are immediately lost. This is depicted in the second part of Fig. 2, where two orbits with pitch angle  $65^\circ$  and  $66^\circ$  are shown. The one at  $65^\circ$  is completely passing and the other is trapped and lost. From orbit calculations it follows that, for energetic ions in W7-AS, it suffices to use the terms passing and trapped (not confined).

### **III. Measurement Technique**

The escaping energetic ions are detected by a probe that is a magnetic spectrometer, as illustrated schematically in Fig. 3. The design follows the concept used for an alpha particle loss diagnostic in TFTR[3,4]. The probe is located outside the plasma, and consists of a metal box with a pair of apertures mounted in one side. Escaping ions that

are able to pass through both apertures strike the end of the box at a position determined by their pitch angle and gyroradius. The end of the box contains a plate coated with a scintillating material that emits light when bombarded by the ions. The image of the light pattern on the scintillator screen is transferred by a series of lenses to detectors that can record the total intensity of light produced and the distribution in gyroradius and pitch angle. A schematic view of the probe, optics, and detectors is shown in Fig. 4.

The details of the deposition pattern of energetic ions are determined by the dimensions of the apertures, their positions relative to the scintillator, and by the orientation of the detector relative to the magnetic field. Ideally, the detector should be oriented such that the local magnetic field lies in the plane of the scintillator. The probe can detect a wide range in pitch angle if: (1) the centerline of the aperture set lies approximately midway between fully parallel and fully perpendicular to the local magnetic field; (2) the rear aperture is wide compared to the front; and (3) the exterior of the probe is shaped to minimize interception of the ion orbits entering the detector. Furthermore, with a sufficiently large scintillator, it is possible to configure a detector system utilizing two sets of apertures and detect co- and counter-going fast ion loss simultaneously. The probe for W7-AS does, in fact, is capable of doing both: cover a wide range of pitch angles and measure particles coming from both directions.

#### **IV. Details of the Detector**

The fast ion loss probe is mounted on top of the device, and its position is shown in Fig.

1. Since the usual operation of the machine is with the toroidal field pointing counterclockwise when seen from above, the ion grad-B and curvature drifts are upward and ions drift toward the probe.

A more detailed diagram of the probe head is shown in Fig. 5. The probe head is cylindrical, with a diameter of 59 mm, but has two flat sides in which the apertures are embedded. These sides are oriented at  $31.2^\circ$  with respect to the local magnetic field direction under normal operation and face away from the axis of symmetry of the machine. The apertures have an apex angle of  $85^\circ$ , allowing particles from  $\sim 10^\circ$  to  $\sim 85^\circ$ , both co- and counter-going, to be detected.

The probe is located at a major radius of 208.6 cm, at a toroidal angle of  $27.8^\circ$  from the middle of field period 3 of W7-AS. Each period subtends  $72^\circ$  toroidally. The probe is mounted on a probe drive system using a bellows that allows it to be moved vertically to as low as 27 cm above the midplane. At the probe location, the vessel wall is at 40 cm above the midplane, so useful detector positions are within this range. The port on which the probe is mounted is equipped with a gate valve so that the probe can be mounted and dismounted without need to vent the main vessel. Its location is near the point (toroidal angle of  $36^\circ$ ) where the plasma cross-section is approximately elliptical with a vertical elongation. In the vicinity of this region, the gradient in the magnetic field is radially inward, so that the ion grad-B and curvature drifts are directed upward toward the probe location. Guiding center orbit calculations for beam ions in W7-AS, done with the



FAFNER code[11], indicated that this is the location of the largest flux of beam ions striking the vessel wall.

The detector response can be modeled numerically, both with the code used to simulate the detectors in TFTR [3] and with a code independently developed for this detector. The results of both are identical, and allow the generation of a mapping between locations on the scintillator and the gyroradius and pitch angle of particles that can strike there. Figure 6a depicts the results of such a numerical simulation, showing the resultant grid of centroids in gyroradius and pitch angle at the scintillator. Note that, in this work, what we term the "gyroradius" is what would be the gyroradius if the particle's motion were fully perpendicular to the field line:  $\rho = (2E/m)^{1/2}/\omega_c$ , where  $E$  is the ion's energy,  $m$  is its mass, and  $\omega_c$  is its cyclotron frequency at the position of the probe. This convention makes the gyroradius independent of pitch angle and simply a measure of the ion's energy. It is not, however, the actual radius of gyration of the particle's orbit.

Figure 6b shows the distributions that arise on the scintillator, as computed by the detector model, for ions at a  $50^\circ$  pitch angle and gyroradii of 1, 2, 3, 4, and 5 cm. These distributions show the significant broadening that is induced by the finite size of the apertures even for a monoenergetic distribution, which introduces considerable uncertainty in any effort to extract the escaping ion energy distribution from the detector signal. The aperture system was designed, at its low energy limit, to be able to pass hydrogen ions at one-third of the injection energy (i.e. 18 keV) at the maximum field of

2.5 T. These particles have a gyroradius of 0.75 cm. Figure 6c shows the instrumental width in pitch angle for particles of a gyroradius of 2 cm. The FWHM varies from  $2^\circ$ - $4^\circ$ .

The scintillator used in the detector is ZnS:Ag (P11), which is quite bright and emits in the blue portion of the spectrum. The light emitted by the scintillator is detected by an intensified video camera (Proscan, 2-inch intensifier) and by an array of photomultipliers (hereafter PMTs, EMI model 9558QA). The overall configuration of the detectors and optics are shown in Fig. 5.

The intensified CCD camera used is water-cooled and has a 14-bit digitizer, allowing finely resolved measurements to be taken. The CCD itself consists of an array of  $512 \times 512$  pixels. However, the sensor read-out to the controlling computer is slow and so the camera must be operated in a mode which averages  $4 \times 4$  pixels, giving an output image  $128 \times 128$  every 100 ms (75 ms minimum). The typical duration of auxiliary heating in W7-AS discharges is from 200 to 900 ms, so this frame capture rate is sufficient to give several images within one discharge. An image of the scintillator from a typical discharge is described in the next section.

The PMTs receive light from individual fiber optic cables (1.5 mm diameter) placed in the image plane of the probe optics. In this way, a fast time-history of the loss at selected pitch angles and gyroradii can be measured. Figure 7 shows data for selected PMTs in a typical shot. Under ordinary conditions, the PMT signals are digitized at 4 kHz.

The scintillator substrate is a glass plate, and it has two domains where a thin layer of Cr has been vapor-deposited before the scintillator powder was applied. These domains correspond to where the co- and counter-going ions strike the scintillator. They are each contacted by the center conductor of a coaxial cable that carries the collected charge outside the vessel where it can be detected. Thus, the probe can also act as a Faraday cup detector[12, 13]. This is particularly convenient for making an absolute ion flux measurement and an absolute calibration of the CCD camera, since even currents as low as a few nA can be measured. Otherwise, absolute calibration of the system would require measuring the luminosity of the scintillator when exposed to a known flux of ions at the beam injection energy, and also measurement by the camera of a light source of known absolute luminosity placed at the scintillator location. Unfortunately, the Cr layer which forms the Faraday cups is mostly transparent, and some light excited by lost ions is transmitted through it, reflects from the back surface of the glass backing plate, and is detected by the CCD camera. The net effect is a broadening of the instrument's response in pitch angle and gyroradius (see example in Sec. V).

Each Faraday cup current was measured using a galvanically isolated current-to-voltage converter ( $I_{\text{max}} = 60 \text{ nA}$ ). The input was biased to a potential of +6 V in order to suppress secondary electron emission. First measurements, however, have shown that at full field (2.5 T) these currents are rather low (less than 10 nA) and that the signals become very noisy and even shift toward negative values when the probe is located close to the plasma edge. This effect was considerably enhanced during ECRH-discharges. In order to overcome these problems the bias voltage had to be removed and the electronic setup was

improved with respect to RF-interference (shot no. > #47094). This led finally to more reliable current measurements ( $I_{\max} = 100 \text{ nA}$ ).

Another important element in calibration of this type of probe is determining the exact position and size of the scintillator within the camera field of view. This knowledge is required in order to map correctly the pitch angle and gyroradius grid determined by the numerical simulations discussed above. Light from plasma-generated X-rays can often help to make this calibration. However, in the W7-AS probe, we have installed three small light bulbs near the scintillator to illuminate it for this calibration. The system uses bulbs selected to have no plastic elements and a minimum amount of attached solder so as to be vacuum compatible. A baffle ring between the lamps and the optics prevents the camera from viewing the lights directly.

## **V. Initial Results**

The energetic ion loss detection probe for W7-AS was first operational in March 1999. In general, the interpretation of the data is complicated by ion orbit shadow effects of protruding in-vessel components, whose effects are determined by ion orbit calculations. In particular, the top rail limiter, located in the vicinity of the probe, can intercept losses of the co-going ions headed for the probe, provided the plasma is limited by the rail limiter and the probe is positioned far from the plasma edge. Such shadow effects depend on the probe position relative to the plasma edge and on the ion energy, since the cross-

field drift speed depends upon particle energy. The shadow effect is often less significant for trapped ions, which are bouncing in the local magnetic mirror at the probe location without making very large excursions in the toroidal direction, depending on the field configuration.

At first, tests were performed utilizing the diagnostic NBI, usually used for charge exchange diagnostics. The injector is located in the same field period at the opposite port of the probe with respect to the underlying stellarator symmetry. The neutral beam is injected at the bottom of the machine in vertical direction with a nominal acceleration voltage of 34 kV, leading to production of trapped fast ions only. If such ions are born below the equatorial plane, they may drift towards the magnetic axis, where the field ripple is low, and enter the adjacent half field period where they can become trapped again. The upward drift motion, finally, leads to losses in the region of the probe location. Thus, the diagnostic NBI serves as a perfect test facility for the probe.

Fig. 7a shows some global plasma parameters and the probe output as a function of time in an ECR-heated plasma at full field (#48225,  $B_{\text{mod}} = 2.5$  T) with a density ramp after 300 ms. The rotational transform at the edge is around  $\iota = 5/9$  leading to a formation of boundary islands [14]. The core plasma in this configuration has a minor radius  $a_{\text{eff}} = 13$  cm, smaller than in limiter configurations ( $a_{\text{eff}} < 18$  cm). During the discharge the diagnostic neutral beam was injected as indicated by the shaded intervals, in which the specified power is only a nominal value. The real power injected into the plasma is estimated to be only a few tens of kilowatts, so that the diagnostic beam does not perturb

the plasma. At least up to 600 ms the discharge appears to be MHD-quiescent as can be assessed from the  $H_\alpha$ -signal. The PMT data are shown only for two specific channels, which are the only ones containing significant signals. In particular, on channel 11 a strong signal is observed covering the full dynamic range of the setup with an excellent signal to noise ratio. A small signal is also observed at channel 14, but the signals of all other channels do not exceed the noise level. Both channels 11 and 14 indicate losses during neutral beam injection only. The fact that the signal strength decreases with density and lower temperature is consistent with slowing down of fast ions, where ion scattering becomes more important under these conditions and thereby fewer ions on direct orbits to the probe are present. It is also evident that after 600 ms the  $H_\alpha$ -signal is no longer quiescent and the apparent noise on the loss signal increases, which is several orders of magnitude larger than the real instrumental noise.

Ion losses during neutral beam injection are also found in cup current time traces up to a level of 15 nA, which is of course a rather low value. The noise level during the discharge amounts to approximately 5 nA, so that the signal to noise ratio is rather poor in comparison to the optical system. Furthermore, this noise level increases when the probe is positioned closer to the plasma edge as discussed in the previous section. Here, the distance between probe and plasma is rather large ( $Z_{\text{probe}} = 38$  cm,  $Z_{\text{limiter}} = 34$  cm,  $Z_{\text{separatrix}} = 22$  cm) and the noise level during the discharge is only slightly above the amplifier noise. It is interesting to compare the absolute loss rates with the intensity of the fast neutral particle source. Although the absolute beam strength is not known exactly, it can be estimated with only a few reasonable assumptions. These include the current

density distribution of neutral hydrogen atoms with the full, half and third of the nominal energy and the beam profile. The neutralizer efficiency and the ion extraction current leads to neutral beam current densities in the order of  $100 \mu\text{A}/\text{mm}^2$  which is much larger than the measured  $25 \text{ nA}/\text{mm}^2$  (aperture size  $0.6 \text{ mm} \times 1 \text{ mm}$ ). The fact that the measured beam loss current density is much lower than the injection density is quite reasonable, since most of the beam will be absorbed in the interior of the plasma and even those portions of the beam that are lost will be spread over a much larger area than just the probe location.

Both PMT and current data reveal losses only from the counter direction. This can be explained with the  $B_{\text{mod}}$  - structure of the field and the lower sensitivity to co-going losses. The reason for choosing such a magnetic configuration at high  $\iota$  is that, due to an enhanced field ripple, beam ions predominately enter the half field period containing the probe rather than the half period in the opposite direction. The CCD data in Fig. 7b, recorded during the indicated time interval (200 - 232 ms) of the same shot depicted in Fig. 7a, also exhibit losses exclusively for counter-going ions. Their distribution is well localized in a small area with a centroid at  $\rho = 11 \text{ mm}$  and pitch angle of  $76^\circ$ . The gyroradius of ions having the full energy is 10.6 mm, which fits quite well with the measurement. Of course, losses of ions with lower energies are also expected, but they are suppressed by the rapidly falling transmission probability of the apertures towards lower gyroradii and by the fact that the slowing down rate of the ions increases with lower energies. It should be noticed also that the CCD data have an excellent signal to noise ratio. The resolution of the system, however, is not sufficient to discriminate

between the full, half and third energy component of the beam, since the energy separation is close to the instrumental resolution, which is in this case slightly reduced by the optical system whose focus is optimized for  $Z_{\text{probe}} = 33$  cm. It is also suspected that the scintillator plate has a halo effect (described in the previous section) leading to an additional broadening of the distribution, since the observed distribution covers regions of the scintillator plate where orbit modeling indicates no ions should be capable of reaching. Taking into account reflections from the backside of the plate, a distribution  $f(r) \sim 1/(1+r^2)$  can be derived, with  $r$  being distance between ion strike point and observation point. The contours, in fact, show such a distribution, very broad at low levels but at high levels narrow contours.

The most relevant result from the data of this shot is that the loss probe is sensitive to fast ions exclusively and that no signal due to stray light, entering the probe through the aperture system, has been observed.

Although the optical and current signals in the presented example are satisfactory, the current signals are often very low ( $< 10$  nA) in discharges with tangential NBI at full field (2.5 T) whereas the sensitivity of the optical system is still sufficient. The loss rates, however, increase rapidly with lower field strength. Therefore an example with co-NBI at half field is presented in Fig. 8a (#46982), exhibiting some interesting features of ion losses during tangential injection. Again, some of the most relevant global plasma parameters and some probe signals are included. The plasma is heated with only one ( $D_0$ ) co-injecting beam source to retain the density at a low level. The density is, nevertheless,



rising during the discharge. The central electron temperature and the plasma stored energy remain almost constant throughout. A selected set of PMT traces are shown, where channel 7 corresponds to low pitch angle and large gyroradii on the co-side and channel 1 and 15 to large pitch angle on the co- and the counter-side, respectively. The video image in Fig. 8b reveals that the loss distribution is separated into three domains. The most intense part corresponds to direct losses matching the mean pitch angle of beam ions around  $30^\circ$  and a gyroradius of 38 mm as obtained by the FAFNER-code [11]. The other losses at large pitch angle show the interesting feature that, although the beam is injected tangentially, trapped ion losses occur. This indicates that pitch angle scattering has to be taken into account, since obviously during the slowing down of them some of the fast ions are scattered into the loss cone of the field configuration. In fact, the centroids of these distributions appear to be shifted to gyroradii below that corresponding to the injection energy, showing that the scattered ions have already suffered a deceleration. The slow change of the signal amplitudes with time can be related to the increase in density, so that ion scattering is more likely. Thus, the fraction of trapped ion losses increases and the direct losses drop with time. Such variations, on time scales larger than the slowing down time, have been observed in a large variety of discharges.

The loss rates are sufficient to obtain cup currents on both co- and counter-side with amplitudes up to the saturation level of the setup (60 nA). In contradiction to the expectation, the counter-current exceeds the co-current at the early stages of the NB heating ( $t > 150$  ms). This, however, cannot be directly observed in video image.

Although a fraction of the direct co-losses is overlapping on the counter-domain (see Fig.

8b) caused by the large gyroradii and the broad instrument function (section IV), the ratio of total co- to total counter-intensities, which were derived by summing up the CCD-intensity over the scintillator domains, is almost constant at  $3/2$ . Here, we encounter the general problem that one has to consider the scintillator light yield with respect to the ion energy. This yield depends linearly on the ion energy, provided that the power deposited by striking ions does not exceed the saturation level of the detector[15]. Losses can be detected down to  $\rho = 5$  mm, which corresponds to 1 keV deuterium in this discharge, close to the thermal energy of the central plasma ions. The light yield varies then by almost two orders of magnitude ( $E_{\text{beam}} = 55$  keV). Small changes in the energy distribution suffice then to alter the ratio of light to current output. Especially when shadow effects of the top rail limiter on the co-side are taken into account, only counter-going low energetic ions can reach the probe. For an absolute calibration of the losses CCD-intensities should be scaled with the ion energy, provided that only losses of one ion species exist.

These examples clearly demonstrate that losses of co- and counter-going ions can be measured simultaneously, which is a new feature of this probe. Only at large gyroradii and low pitch angle loss distributions of co- and counter-going ions may overlap. In those cases co- and counter-losses can be discriminated by varying the probe position and taking advantage of shadow effects of protruding built-in parts.

## VI. Summary

In conclusion, we have constructed a fast ion loss probe for W7-AS. It is capable of measuring a wide range of pitch angle, and of measuring both co- and counter-going fast ion loss simultaneously.

## Acknowledgements

One author (DD) appreciates the hospitality shown by the W7-AS team during several visits to IPP. We are also grateful to Dr. K. Young of PPPL for his support of this effort. This work was supported in part by US DoE contract number DE-AC02-76CH03073.

## References:

- [1] G. Grieger, *et al.*, *J. Plasma Fusion Res. SERIES* **1**, 53-56 (1998).
- [2] M. Fujiwara, *et al.*, *J. Plasma Fusion Res. SERIES* **1**, 57-61 (1998).
- [3] S. J. Zweben, *et al.*, *Nucl. Fusion* **30**, 1551 (1990).
- [4] D. S. Darrow, *et al.*, *Rev. Sci. Instrum.* **66**, 476 (1995).
- [5] D. S. Darrow, *et al.*, *J. Plasma Fusion Res. SERIES* **1**, 362-365 (1998).
- [6] J. Rome, *Nucl. Fusion* **35**, 195 (1995).
- [7] ) S.A. Dettrick, S.S. Lloyd, H.J. Gardner, R.L. Dewar and S.L. Painter, *Nucl. Fus.*, **38**(7), 1001-1012 (1998).
- [8] G. Grieger , *et al*, *Phys. Fluids B*, **4** , 2081-2091 (1992)

- [9] U. Brossmann, *et al.*, *Nucl. Fusion Suppl. (Proc. 9<sup>th</sup> Int. Conf. on Plasma Phys. and Control. Nucl. Fusion Res.*, Baltimore, 1982), vol. III, 141 (1983).
- [10] H. Renner, *et al.*, *Plasma Phys. Control. Fusion* **31**, 1579 (1989).
- [11] F.-P. Penningsfeld, 11<sup>th</sup> Conf. on Control. Fusion and Plasma Phys. *EPS Conference Abstracts* **7**, 323 (1983).
- [12] F. E. Cecil, *et al.*, *Rev. Sci. Instrum.* **70**, 1149-1153 (1999).
- [13] D. S. Darrow, *et al.*, *Rev. Sci. Instrum.* **70**, 838-840 (1999).
- [14] K McCormick *et al.*, *Plasma Phys. Control. Fusion* **41**, B285-B304 (1999)
- [15] M Tuszewski and S J Zweben, *Rev. Sci. Instrum.* **63**, 4542-4544 (1992)

### Figure Captions:

Fig. 1: A top view of the W7-AS device, showing the magnetic field coils, the eight neutral beam injectors, and the probe location. The major radius of the W7-AS chamber is 2.08 m.

Fig. 2: Orbits of 5 keV and 50 keV  $H^+$  ions in a W7-AS magnetic equilibrium which has  $\iota=0.34$ . The top figure displays the orbits in toroidal angle ( $\phi$ ) and poloidal angle ( $\theta$ ). Contours of  $|B|$  at  $r = 11\text{cm}$  are included. In the lower left, the same orbits for 5 keV  $H^+$  ions with pitch angles  $0^\circ$ ,  $72^\circ$  and  $80^\circ$  are shown, plotted in flux coordinates. In

the lower right, orbits for 50 keV  $H^+$  ions with pitch angles  $0^\circ$ ,  $65^\circ$  and  $66^\circ$  are shown.

Fig. 3: A schematic of top and side view of probe operation, including a fast ion orbit.

The gyroradius (energy) of the particle determines how far from the apertures it will strike the scintillator. The pitch angle determines where the ion will strike along the orthogonal dimension of the scintillator.

Fig. 4: An overall diagram of the W7-AS fast ion loss probe, including the scintillator, lamps, movable probe shaft, optics, CCD camera, optical fibers, etc.

Fig. 5: An isometric line diagram of W7-AS probe head, including the scintillator, metal film domains for charge collection, apertures, and supporting structures. The aperture "cones" are at the right hand side in this view.

Fig. 6a: The pitch angle and gyroradius centroid maps for a typical condition in W7-AS.

Maps for both co and counter-going apertures are shown, along with the outlines of the scintillator substrate and the Cr film coated areas. Values of the gyroradius and pitch angle intervals are indicated on the counter map only.

Fig. 6b: The modeled gyroradius centroid distributions for 1, 2, 3, 4, & 5 cm at a pitch angle of  $50^\circ$ . The distributions get broader at large gyroradius because the particles strike the scintillator progressively further from normal incidence, in which case the

apertures have less and less collimating effect. The curves represent the result from a numerical simulation of the detector with equal numbers of ions at each gyroradius.

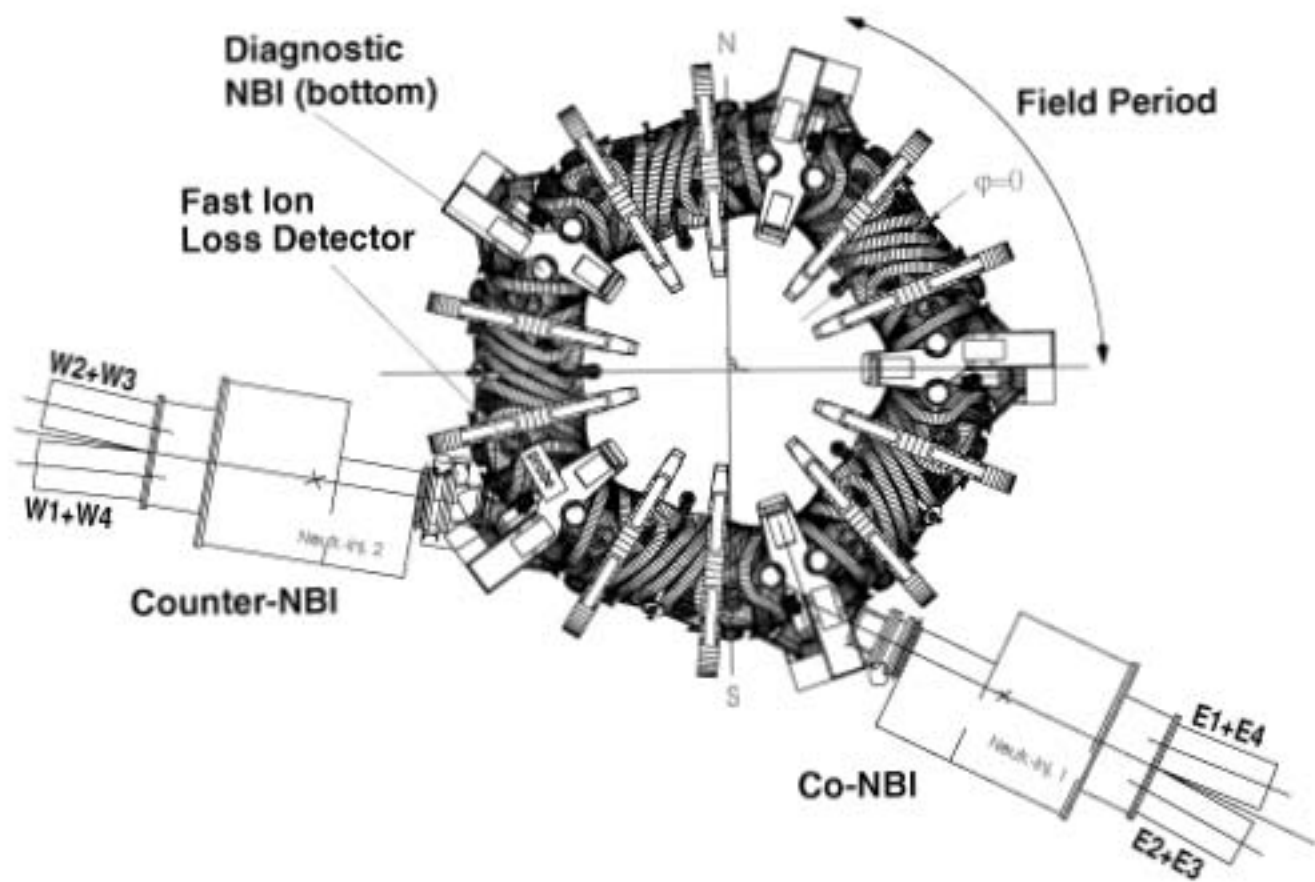
Fig. 6c: The modeled pitch angle distributions for  $20^\circ$ ,  $40^\circ$ ,  $60^\circ$ , &  $80^\circ$  at a gyroradius of 2 cm. The curves represent the result from a numerical simulation of the detector with equal numbers of ions at each pitch angle.

Fig. 7a: Time histories of some global plasma parameters of shot #48225 (ECRH + perpendicular NBI). The loss probe signals are shown for two PMT channels, both observing counter losses at high pitch angle, and the current output of the Faraday cup.

Fig. 7b: Video image of the scintillator output of shot 48225 at 200 - 232 ms overlaid with calculated grids. Lines of constant gyroradius are at 5, 7.5, 10, 15, 20, 25, 30, 35, 40, 50 mm, lines of constant pitch angle from  $20^\circ$  to  $85^\circ$  in steps of  $5^\circ$ . The areas observed by PMTs are indicated.

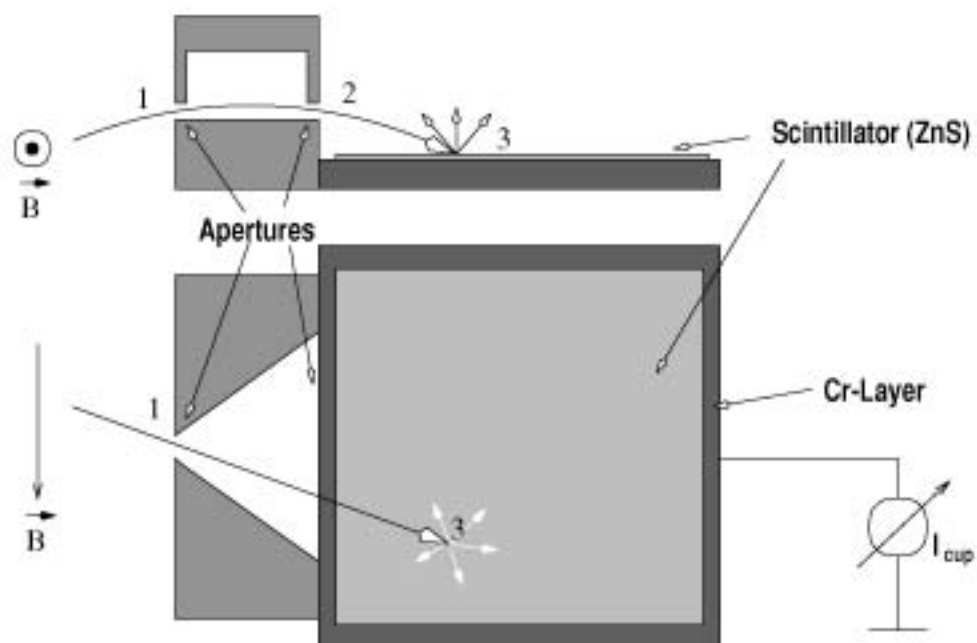
Fig. 8a: Same as Fig. 7a for shot #46982 (tangential NBI) with PMT channels 1 (co, high pitch angle), 7 (co, low pitch angle) and channel 15 (counter, high pitch angle).

Fig. 8b: Same as Fig. 7b for shot #46982.

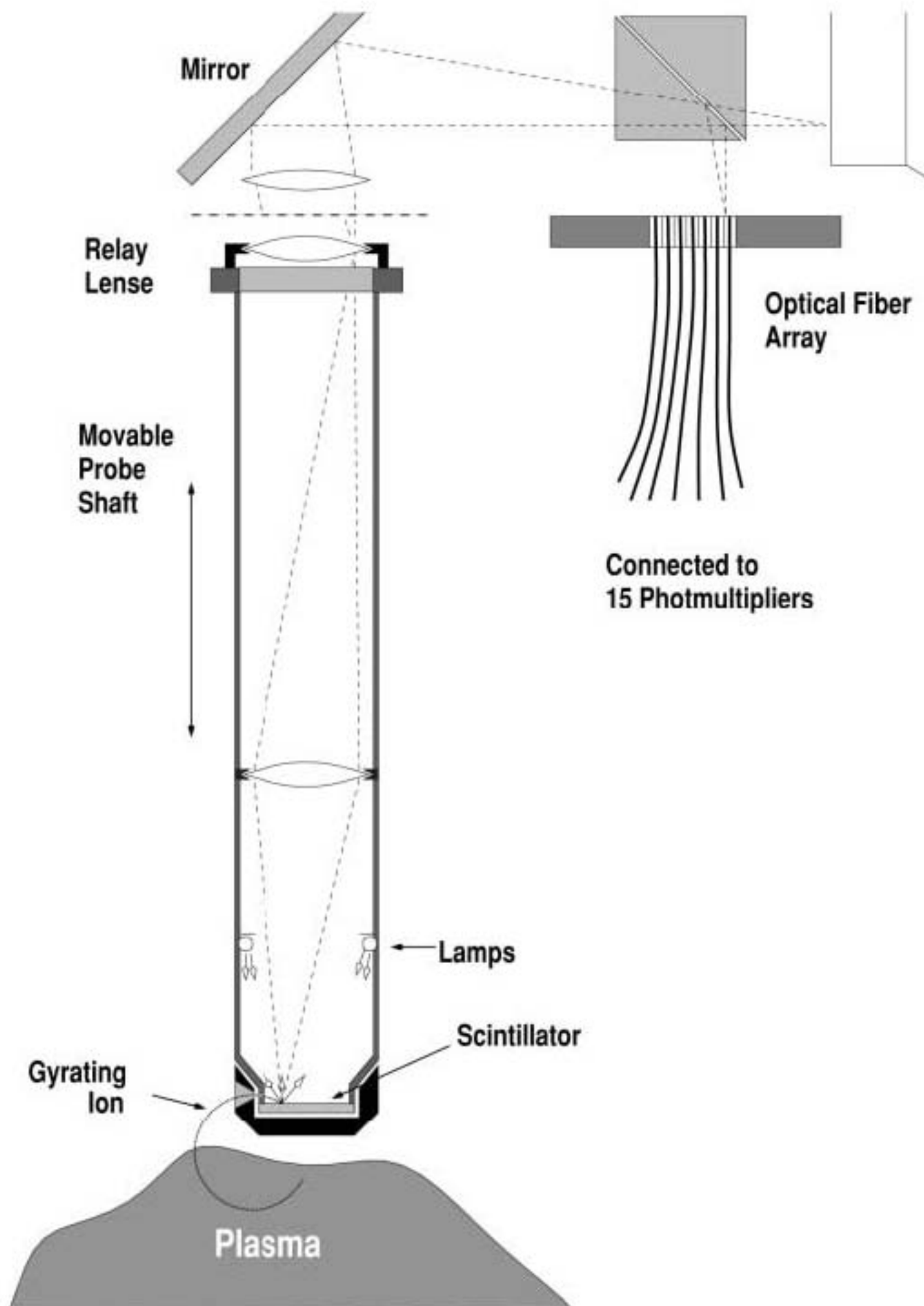


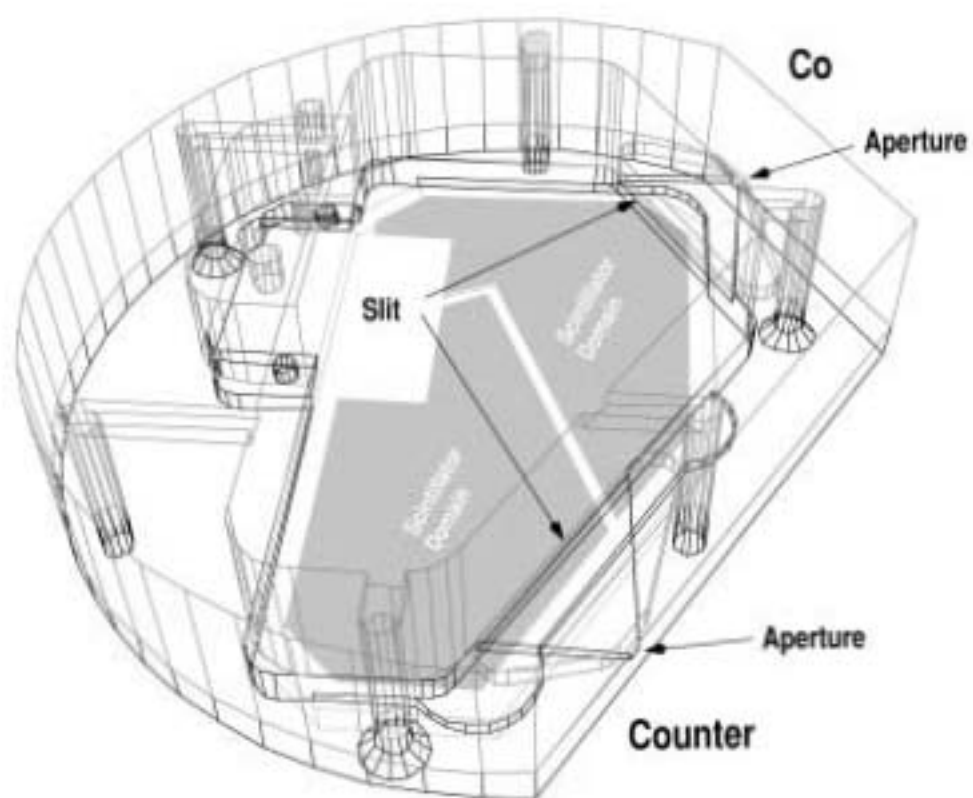


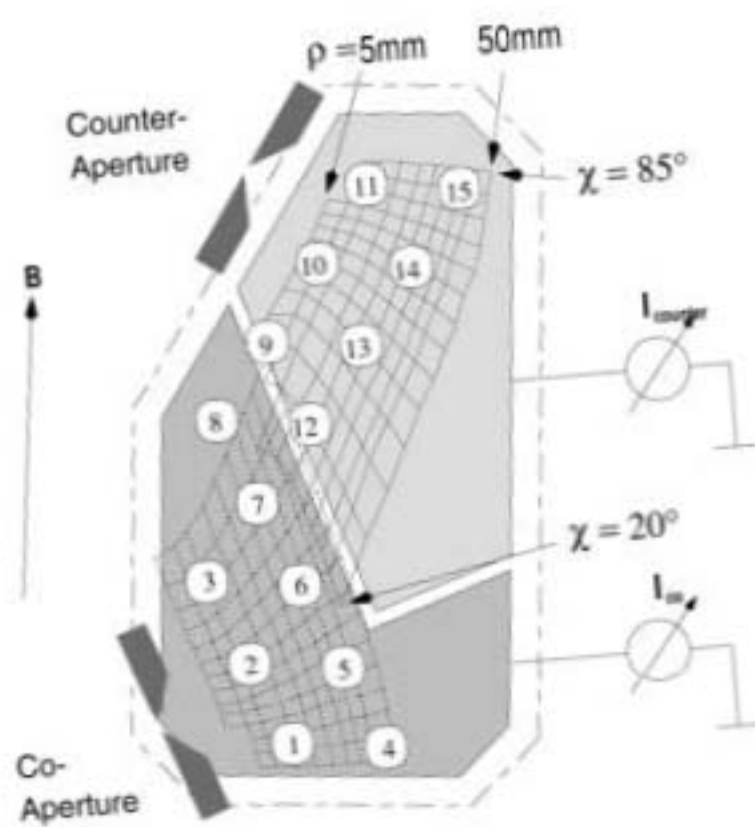


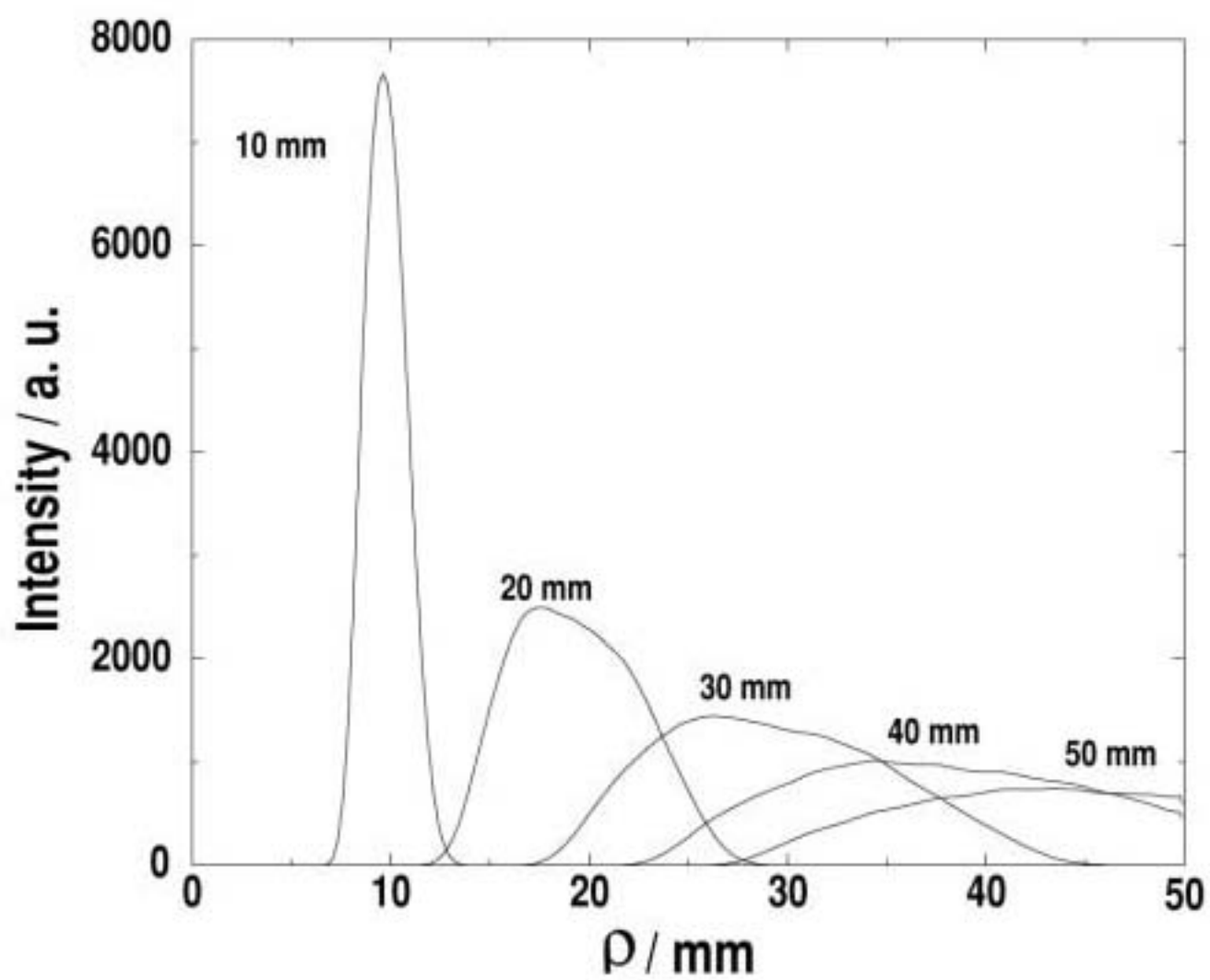


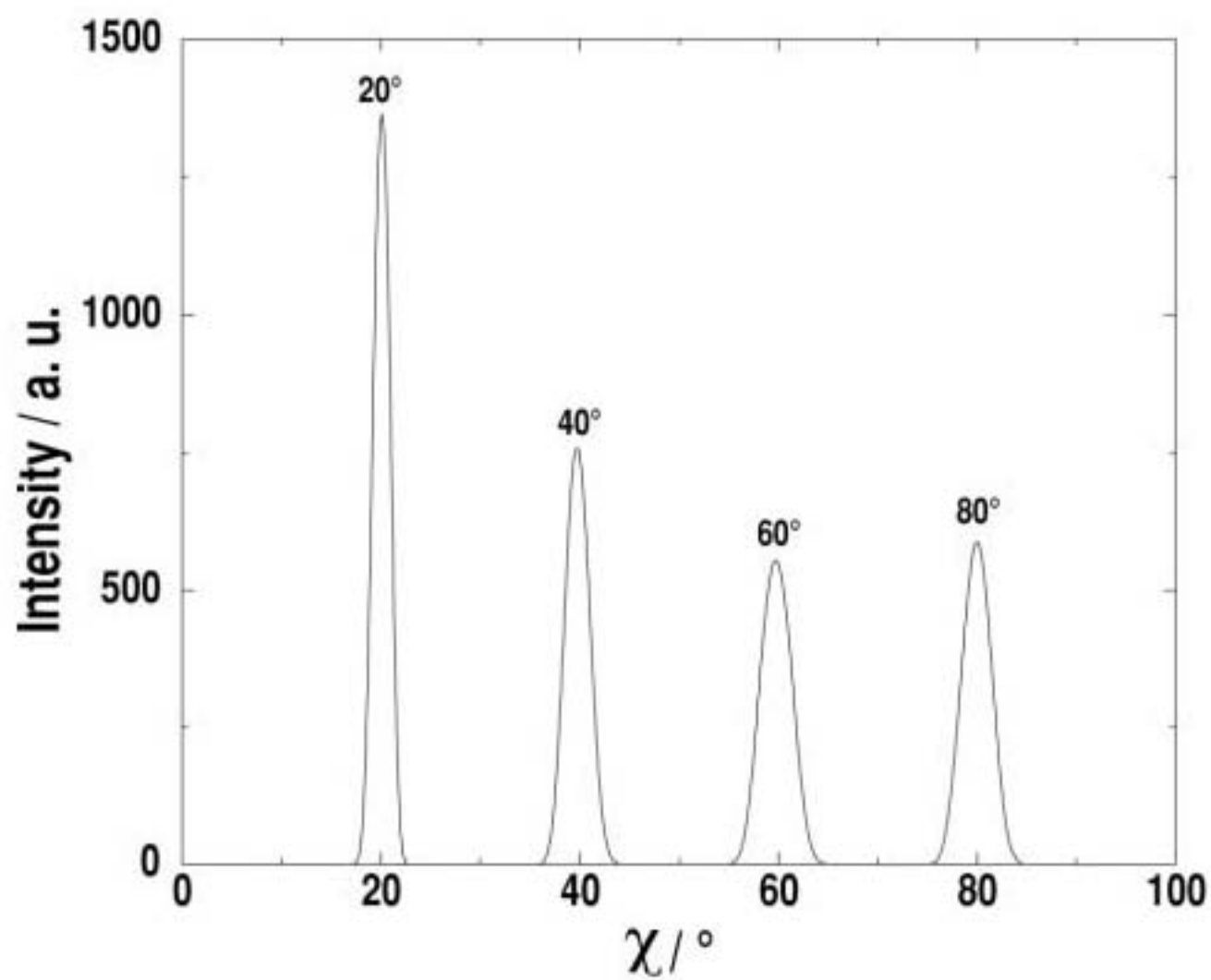
Points 1,2 and 3 => gyroradius  
 Points 1 and 3 => pitch angle



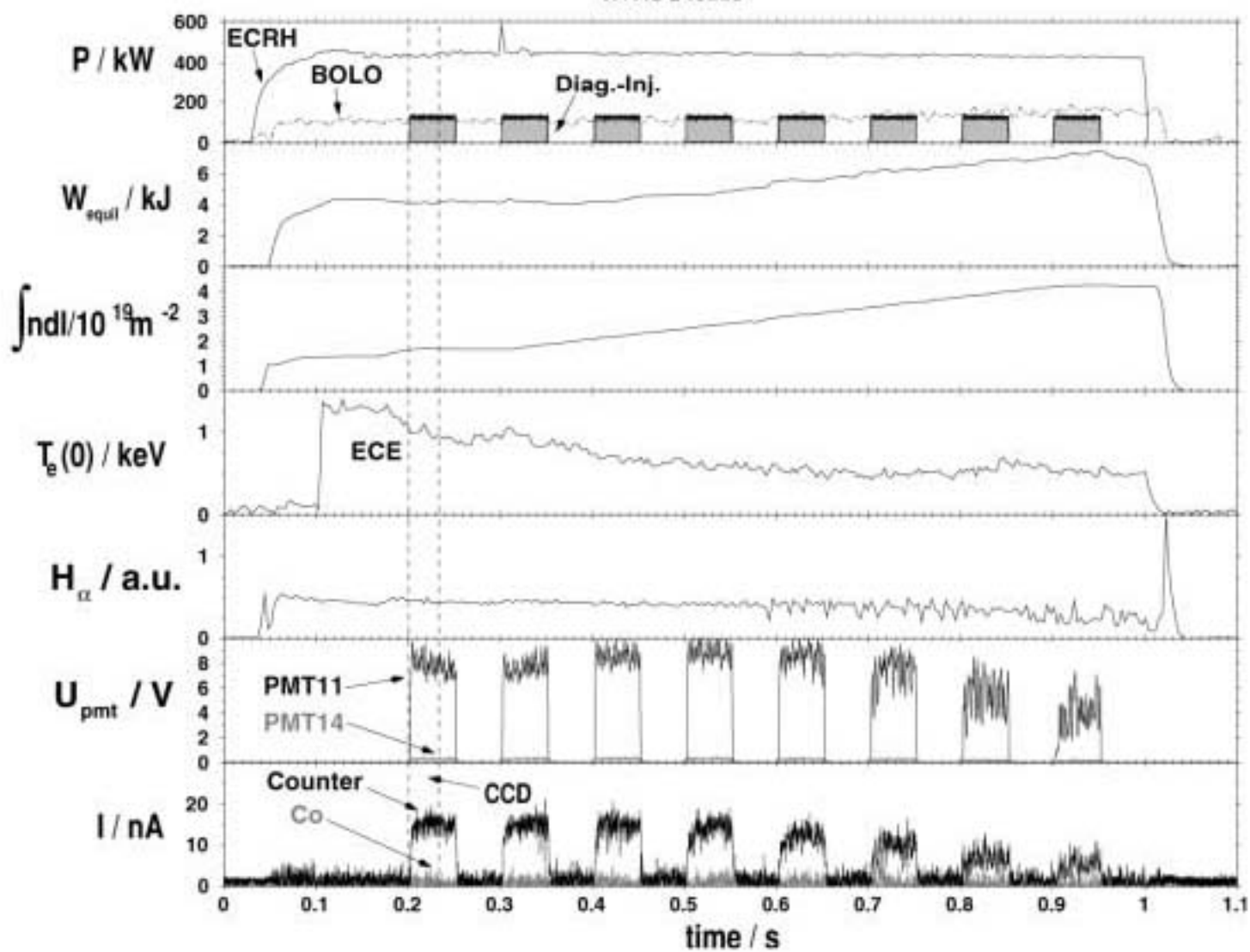




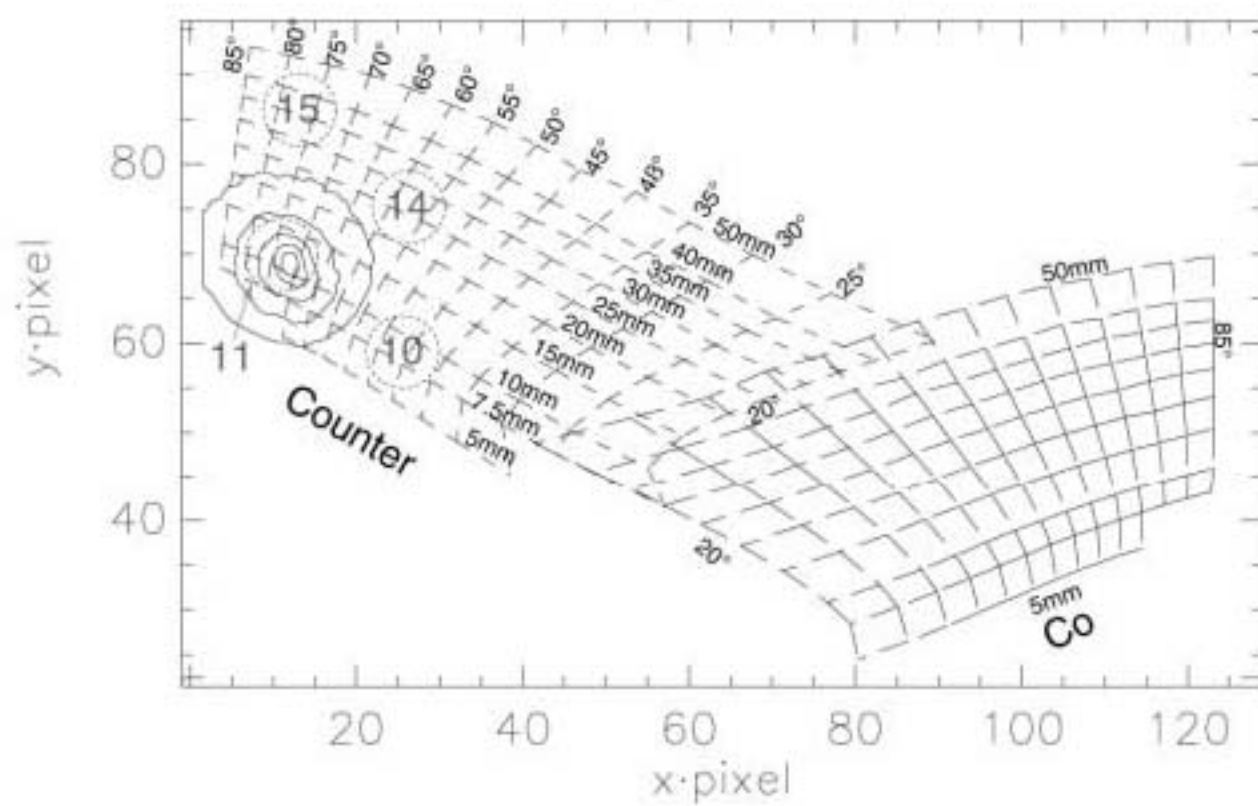




W7AS #48225

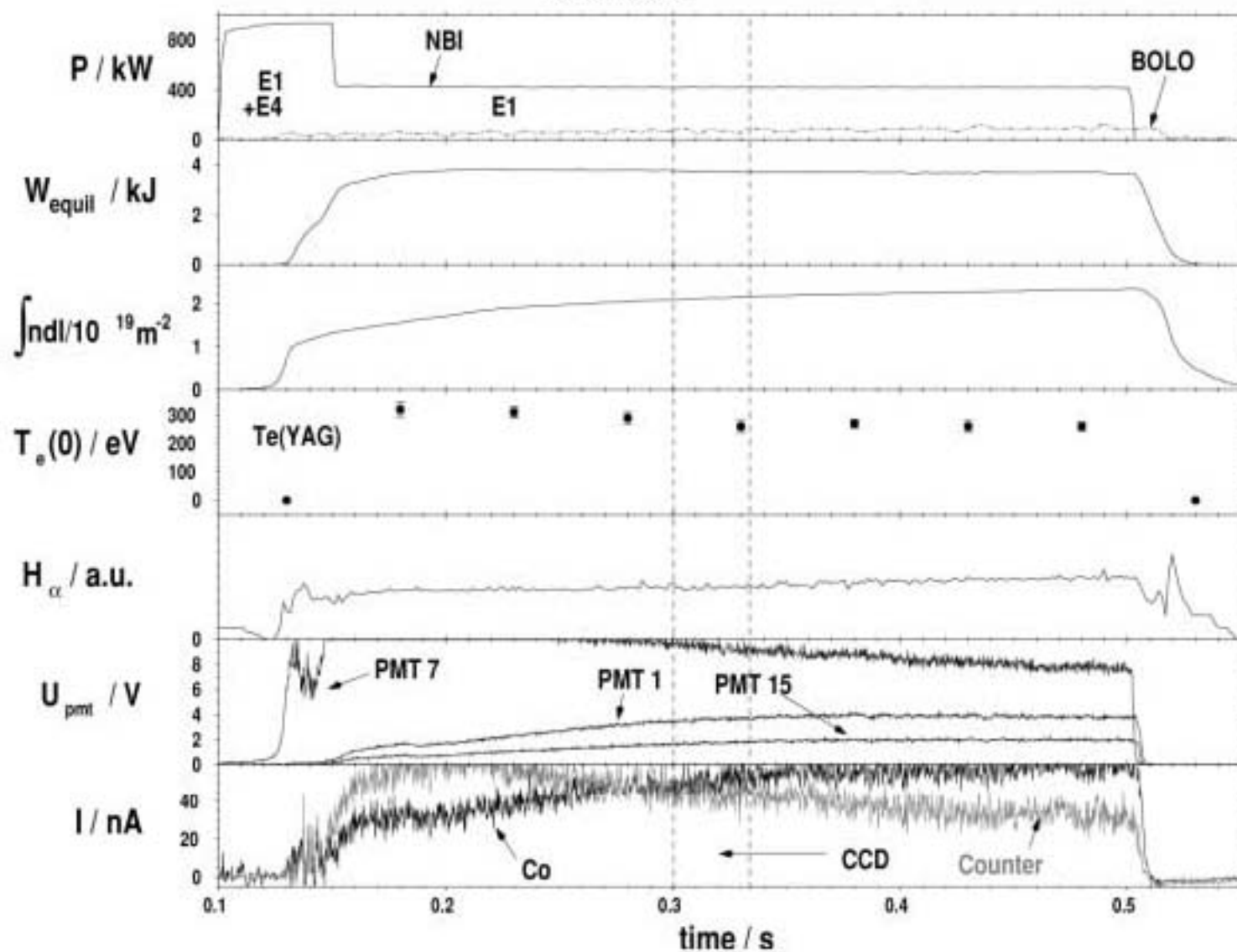


CCD Image :48225.psi

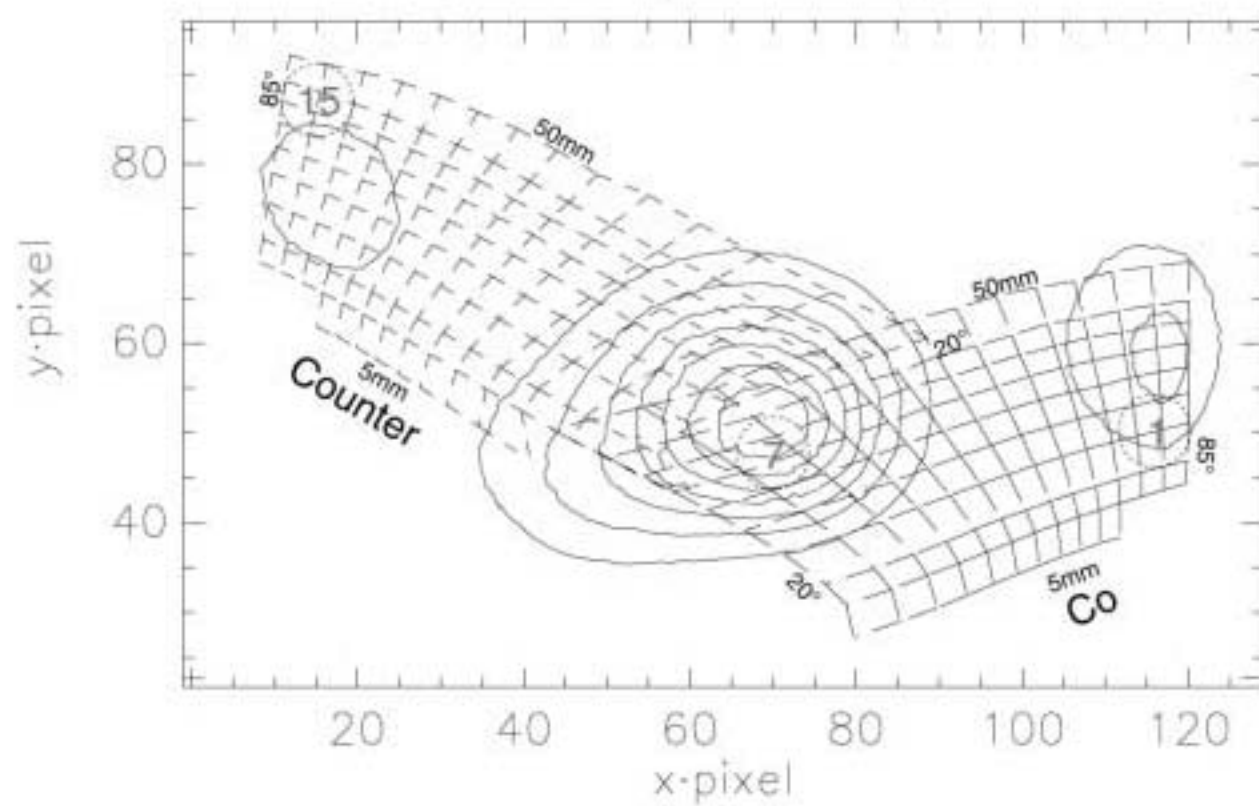




W7AS #46982



CCD Image :46982.psi



The Princeton Plasma Physics Laboratory is operated  
by Princeton University under contract  
with the U.S. Department of Energy.

Information Services  
Princeton Plasma Physics Laboratory  
P.O. Box 451  
Princeton, NJ 08543

Phone: 609-243-2750  
Fax: 609-243-2751  
e-mail: [pppl\\_info@pppl.gov](mailto:pppl_info@pppl.gov)  
Internet Address: <http://www.pppl.gov>